Collapse of a bubble in an electric field

P. D. M. Spelt and O. K. Matar
Department of Chemical Engineering, Imperial College London, South Kensington Campus, London SW7 2AZ, United Kingdom
(Received 19 May 2006; published 27 October 2006)

A low-Mach-number analysis is presented of the collapse of a bubble in an electric field, which is assumed to be homogeneous, but may be unsteady. Ellipsoidal shape deformations are accounted for in the analysis, but are assumed to be small. It is shown that the presence of an electric field leads to additional terms in a modified Rayleigh-Plesset equation. This differential equation for the bubble radius and a corresponding equation for ellipsoidal shape deformations have been integrated numerically. The results indicate that a bubble can be made to collapse by instantaneously switching on an electric field. Also, nonharmonic volumetric oscillations are observed for time-dependent electric fields of sufficiently large amplitude. It is shown that the rate of a collapse driven by external pressure variations due, for instance, to acoustic forcing can be accelerated.

DOI: 10.1103/PhysRevE.74.046309 PACS number(s): 47.20.−k, 47.55.D−, 47.85.Dh, 47.55.dp

I. INTRODUCTION

In this paper, we investigate how the application of an electric field changes the dynamics of the collapse of a bubble. Large volumetric oscillations are considered here, thereby generalizing the analysis of Lee and Kang [1], which is restricted to weak deviations from the initial bubble size. These authors studied the effect of an electric field on the frequency at which bubbles oscillate about a steady shape. From this previous work, it is known that bubbles are either larger or smaller when a spatially and temporally uniform electric field is present, depending on the value of the gas pressure in the absence of the electric field. Also, bubbles assume a prolate ellipsoidal shape when exposed to an electric field. The frequency of oscillation associated with shape modes is altered by changes in the steady shape about which the oscillations take place, and also because of a direct effect of the electric field on the oscillations. It is not yet known how such trends carry over to the collapse of a bubble.

The dynamics of a collapsing bubble is detrimental in a variety of applications, including bubble-enhanced sonoporation [2], sonoluminescence [3], cavitation [4], and in attempts to establish sonofusion [5]. In most cases, the collapse is forced solely by changes in the ambient pressure. Additional control of the collapse would therefore be desireable. Furthermore, electric fields are of course known to have a significant effect on the dynamics of bubbles in electrohydrodynamic boiling, dielectrophoresis [6], and are used in a microfluidic bubble-driven pump [7] and as a means to promote bubble detachment from an orifice in microgravity [8].

In this paper, we shall modify the analysis of the collapse of a bubble in an infinite liquid by Prosperetti and Lezzi [9,10] to account for the presence of an electric field. This is a low-Mach-number analysis, which is therefore restricted to cases in which the velocity of the bubble surface is assmued to be small compared to the speed of sound in the liquid. The electric field in both phases will be assumed to be solenoidal and irrotational, thus electric effects enter the problem via the contribution of the Maxwell stresses to the interfacial boundary conditions. The Maxwell stresses are determined by solving an electrostatic description of the electric field for a deformable bubble in a spatially uniform but potentially temporally varying electric field. It will be shown that the inclusion of these stresses in the model description leads to a modified Rayleigh-Plesset-type equation for the bubble radius.

Furthermore, because an electric field deforms the bubble, it is necessary to extend the analysis to account for finite deviations from sphericity. These shape deformations are assumed to be small, such that a linearized analysis can be employed. This assumption is tested *a posteriori*, when presenting the results. The bubble surface is represented using Legendre polynomials, and the kinematic and dynamic interfacial conditions are satisfied in an integral sense by making use of the orthogonality of Legendre polynomials (e.g., Refs. [3,11]).

The rest of this paper is organized as follows. The electric field is determined in Sec. II A. The modified Rayleigh-Plesset equation and the corresponding differential equations for other shape modes are derived in Sec. II B. These equations are integrated numerically and the results are presented in Sec. III. Finally, concluding remarks are provided in Section IV.

II. FORMULATION

A. Electrostatics

We consider the dynamics of a gas bubble of conductivity κ_{in} and dielectric constant ε_{in} in a liquid of conductivity κ and dielectric constant ε, subjected to a spatially uniform but potentially unsteady electric field $\mathbf{E}_0(t)$. In each fluid, it is assumed that there is no free bulk charge, and that the electrical properties are uniform. Under these assumptions, the electric fields $\mathbf{E}$ and $\mathbf{E}_{\text{in}}$ are solenoidal and irrotational, and one can write $(\mathbf{E},\mathbf{E}_{\text{in}})=\nabla(\psi,\psi_{\text{in}})(\mathbf{x},t)$, where ψ and ψ_{in} satisfy Laplace's equation (see, e.g., Ref. [12]); the subscript "in" will be used to designate properties pertaining to the bubble contents. The conditions at the interface are

$$\varepsilon\mathbf{n}\cdot\nabla\psi-\varepsilon_{\text{in}}\mathbf{n}\cdot\nabla\psi_{\text{in}}=q/\varepsilon_0, \tag{1}$$

$$\psi=\psi_{\text{in}}, \tag{2}$$

$$-\kappa \mathbf{n}\cdot\nabla\psi+\kappa_{\text{in}}\mathbf{n}\cdot\nabla\psi_{\text{in}}=-\frac{\partial q}{\partial t}+q(\mathbf{u}\cdot\mathbf{n})\nabla\cdot\mathbf{n}, \tag{3}$$

where $\mathbf{u}$ is the fluid velocity, q is the interfacial charge density, $\mathbf{n}$ is the outward-pointing normal vector to the interface, ε_0 is the permittivity of free space, and t denotes time. These equations correspond to the jump condition for the component of the displacement vector (equal to the surface charge), continuity of the tangential component of the electric field, and the unsteady balance of free charge at the interface, respectively. We note here that, unlike in Ref. [1], we account for transport of charge density along the interface by including the final term in Eq. (3), written in the form proposed in Ref. [13] for the related problem of surfactant transport (see also Ref. [12]).

The analysis by Lee and Kang [1] shows that, for a locally uniform electric field, the dominant shape distortions are ellipsoidal; a similar conclusion has been reached for collapsing bubbles in the absence of an electric field [14]. In this section, we shall restrict our analysis to shape distortions of the form

$$F=R(t)+R_2(t)P_2(\mu)-r=0, \tag{4}$$

where the spherical coordinates (r,θ,φ) are used, $\mu=\cos\theta$, and $P_2(\mu)$ is the Legendre polynomial of degree 2. In the next section, the dominant mode will be shown to be the P_2 mode considered here. The following analysis is linearized with respect to $\epsilon\equiv\hat{R}_2/\hat{R}$, where $\hat{R}$ and $\hat{R}_2$ are typical values of $R(t)$ and $R_2(t)$, respectively. This assumption will be tested *a posteriori*. Since neither the ambient electric field nor the shape distortions create deviations from an axisymmetric electric potential, the solution of Laplace's equation can be written as

$$\psi=(E_0+AR^3/r^3)r\cos\theta+\sum_{k=2}^{\infty}A_kP_k(\cos\theta)/r^{k+1} \tag{5}$$

in the liquid, and

$$\psi_{\text{in}}=Br\cos\theta+\sum_{k=2}^{\infty}B_kr^kP_k(\cos\theta) \tag{6}$$

inside the bubble. Note that we have demanded that ψ and ψ_{in} be regular as $r\to\infty$ and $r\to 0$, respectively. We also express the interfacial charge density as follows:

$$q=\hat{q}\cos\theta+\hat{q}_3P_3(\cos\theta). \tag{7}$$

Here, r and θ are polar coordinates with respect to the unit vector along $\mathbf{E}_0$ (E_0 is the magnitude of $\mathbf{E}_0$). The coefficients in the above expressions for ψ, ψ_{in}, and q are obtained by integrating the interfacial conditions over a unit sphere, after multiplication with a Legendre polynomial, and making use of the orthogonality of the latter. The results are

$$A=\frac{E_0(\varepsilon-\varepsilon_{\text{in}})-\hat{q}/\varepsilon_0}{\varepsilon_{\text{in}}+2\varepsilon}+\frac{R_2}{R}\left(\frac{\frac{4}{5}E_0(\varepsilon_{\text{in}}-\varepsilon)-\frac{2}{5}\hat{q}/\varepsilon_0}{\varepsilon_{\text{in}}+2\varepsilon}+\frac{[E_0(\varepsilon-\varepsilon_{\text{in}})-\hat{q}/\varepsilon_0]\left(2\varepsilon_{\text{in}}+\frac{2}{5}\varepsilon\right)}{(\varepsilon_{\text{in}}+2\varepsilon)^2}\right), \tag{8}$$

$$B=\frac{3\varepsilon E_0-\hat{q}/\varepsilon_0}{\varepsilon_{\text{in}}+2\varepsilon}+\frac{R_2}{R}\left(\frac{-\frac{12}{5}\varepsilon E_0+\frac{4}{5}\hat{q}/\varepsilon_0}{\varepsilon_{\text{in}}+2\varepsilon}+\frac{(3\varepsilon E_0-\hat{q}/\varepsilon_0)\left(2\varepsilon_{\text{in}}+\frac{2}{5}\varepsilon\right)}{(\varepsilon_{\text{in}}+2\varepsilon)^2}\right); \tag{9}$$

the remaining constants follow as

$$A_2=B_2=0, \tag{10}$$

$$A_3(4\varepsilon+3\varepsilon_{\text{in}})/R^5=\frac{6}{5}\varepsilon E_0R_2/R-\hat{q}_3/\varepsilon_0+\frac{6}{5}A(4\varepsilon+3\varepsilon_{\text{in}})R_2/R+\frac{3}{5}B\varepsilon_{\text{in}}R_2/R-\frac{9}{5}E_0\varepsilon_{\text{in}}R_2/R, \tag{11}$$

and

$$B_3(4\varepsilon+3\varepsilon_{\text{in}})R^2=\frac{18}{5}\varepsilon E_0R_2/R-\hat{q}_3/\varepsilon_0-\frac{6}{5}B(\varepsilon_{\text{in}}+2\varepsilon)R_2/R. \tag{12}$$

There are no contributions from $k\geqslant 4$. It has been verified that the terms proportional to R_2 in Eqs. (8), (10), and (11) are in agreement with Eq. (4.54) for $q=0$, $\varepsilon_{\text{in}}=0$ in Ref. [1].

The balance of free charge at the interface, given by Eq. (3), yields

$$-\dot{\hat{q}}=\kappa\left[E_0-2A+\frac{6}{5}(A-E_0)R_2/R\right]-\kappa_{\text{in}}B\left(1-\frac{6}{5}R_2/R\right)+2\hat{q}\dot{R}/R+\frac{24R_2\dot{R}}{15R^2}\hat{q}+\frac{4\hat{q}}{5R}\dot{R}_2 \tag{13}$$

and

$$-\dot{\hat{q}}_3=\frac{6}{5}[\kappa(E_0+4A)-\kappa_{\text{in}}B]R_2/R-4\kappa A_3/R^5-3\kappa_{\text{in}}B_3R^2+2\frac{\dot{R}}{R}\hat{q}_3+\frac{12\dot{R}R_2}{5R^2}\hat{q}+\frac{6\hat{q}}{5R}\dot{R}_2, \tag{14}$$

where $\dot{(\,)}$ denotes differentiation with time. Equation (14) indicates that $\hat{q}_3$ is of $O(\epsilon)$, so products of $\hat{q}_3$ with other terms of that order have been discarded, for consistency.

For future reference, the normal component of the Maxwell stress exerted by the electric field on the bubble is

$$\mathbf{nn}:\mathbf{M}(r) = \varepsilon_0\varepsilon\mathbf{nn}:\left(\mathbf{EE} - \frac{1}{2}|\mathbf{E}|^2\mathbf{I}\right)$$

$$= \varepsilon_0\varepsilon\left(\frac{1}{2}(\psi_r^2 - r^{-2}\psi_\theta^2) - 2\psi_r\psi_\theta\frac{R_2}{r^2}\frac{\partial P_2}{\partial\theta}\right), \quad (15)$$

to be evaluated at $r=R+R_2P_2(\cos\theta)$, where $\mathbf{I}$ is the identity matrix. On the liquid side, this becomes (after linearization in the small parameter R_2/R)

$$(\varepsilon_0\varepsilon)^{-1}\mathbf{nn}:\mathbf{M}^l$$

$$= \frac{1}{2}\{[(E_0-2A)^2 + 12A(E_0-2A)R_2R^{-1}P_2(\cos\theta)]$$

$$\times\cos^2\theta - [(E_0+A)^2 - 6A(E_0+A)R^{-1}R_2P_2(\cos\theta)]$$

$$\times\sin^2\theta\} - 6\frac{R_2}{R}(E_0+A)(E_0-2A)\sin^2\theta\cos^2\theta$$

$$- 4(E_0-2A)A_3\cos\theta P_3(\cos\theta)/R^5 + (E_0+A)A_3$$

$$\times\sin\theta\frac{\partial P_3}{\partial\theta}\Bigg/ R^5. \quad (16)$$

On the gas side,

$$(\varepsilon_0\varepsilon_{\text{in}})^{-1}\mathbf{nn}:\mathbf{M}^g = B^2\left(\cos^2\theta - \frac{1}{2} - 6\frac{R_2}{R}\sin^2\theta\cos^2\theta\right)$$

$$+ 3BB_3R^2\cos\theta P_3(\cos\theta)$$

$$+ BB_3R^2\sin\theta\frac{\partial P_3}{\partial\theta}. \quad (17)$$

It will be shown in the next section that these expressions lead to results that are in agreement with the findings in Ref. [1] for the case of $q=0$, $\varepsilon_{\text{in}}=0$ (to which their analysis is restricted).

B. Modified Rayleigh-Plesset equation

We extend here the low-order theory in a Mach number, $\text{Ma}=U/C$ (where U and C are a characteristic fluid velocity and speed of sound in the liquid) of Prosperetti and Lezzi [9,10], to account for the presence of an electric field. As is clear from Ref. [1], an electric field causes shape oscillations, so it is necessary to drop the assumption of spherical symmetry made in Ref. [9,10]. In the analysis of Ref. [9], viscous effects are only accounted for through a normal viscous stress, where the rate of strain is obtained from the irrotational velocity field. The argument for doing so is that viscous effects enter the momentum equation (in the case of a spherically symmetric bubble) only through the compressibility of the liquid, and are usually small. Brenner *et al.* [15] and Hilgenfeldt *et al.* [14] used a boundary-layer approximation, based on an earlier analysis by Prosperetti [16], to account for viscous effects on shape oscillations. In the present analysis, we shall ignore the viscous terms in the momentum equations and assume the flow to be irrotational, so that the liquid velocity can be written as $\mathbf{u}=\nabla\phi$, but account for the spherically symmetric component of the viscous normal stress. A viscous correction for shape oscillations is introduced at the end of this section, consistent with Ref. [14]. Following the analysis of Ref. [9], we shall assume that the local liquid pressure p is a function of the local density only (barentropic flow). Under these assumptions, it can be shown that [9]

$$\nabla^2\phi = -\frac{1}{c^2}\frac{Dh}{Dt} \quad (18)$$

and

$$h = -\frac{\partial\phi}{\partial t} - \frac{1}{2}|\nabla\phi|^2, \quad (19)$$

where $h=\int_{p_\infty}^{p} dp/\rho$ is the enthalpy and p_∞ is the liquid pressure in the absence of a bubble. Eliminating h from Eq. (18) results in

$$\nabla^2\phi = \frac{1}{c^2}(\phi_{tt} + 2\nabla\phi\cdot\nabla\phi_t + \nabla\phi\nabla\phi:\nabla\nabla\phi). \quad (20)$$

A modified Tait form of the pressure-density relationship for the liquid is used here [9,14],

$$\frac{p+\mathcal{B}}{p_\infty+\mathcal{B}} = \left(\frac{\rho}{\rho_\infty}\right)^n, \quad (21)$$

such that the speed of sound is given by

$$c^2 = \frac{dp}{d\rho} = c_\infty^2 + (n-1)h, \quad (22)$$

where $\mathcal{B}$ is a constant and c_∞ corresponds to the speed of sound in the absence of a bubble. Substitution of c in Eq. (20) gives

$$\nabla^2\phi = \frac{1}{c_\infty^2}\Bigg[\phi_{tt} + 2\nabla\phi\cdot\nabla\phi_t + \nabla\phi\nabla\phi:\nabla\nabla\phi$$

$$+ (n-1)\left(\phi_t + \frac{1}{2}|\nabla\phi|^2\right)\nabla^2\phi\Bigg], \quad (23)$$

where only terms up to c_∞^{-2} have been taken into account.

In order to show which modes will have the most dominant contribution from the electric field, the bubble surface is represented in this section as

$$F = R(t) + R_{kl}(t)Y_{kl}(\mu,\varphi) - r = 0, \quad (24)$$

where $Y_{kl}=P_k^l(\mu)\cos(l\varphi)$ is a surface harmonic, $k>0$, and $-k\leqslant l\leqslant k$. Since $Y_{00}=1$, $R(t)$ corresponds to $R_{00}(t)Y_{00}$, so we have suppressed these additional subscripts here for clarity. The following analysis is linearized with respect to $\epsilon \equiv R_{kl}/R$; this assumption will be tested *a posteriori*. Accordingly, we can write

$$\phi = \phi_0 + \epsilon\phi_1 + \cdots. \quad (25)$$

Prosperetti and Lezzi [9,10] showed that, for a spherical bubble oscillating at relatively low values of M, ϕ_0 in the near and far fields should be considered seperately. In the near field, the spatial coordinates scale with a representative bubble radius, R_c, and t with R_c/U, such that Eq. (23) becomes, to $O(M^2)$,

$$\nabla^2\phi = 0. \tag{26}$$

The near-field solution, governed by Eq. (26), can be written in terms of spherical harmonics. The kinematic condition relates these harmonics to Eq. (24). Since the Y_{kl} are orthogonal, and noting that only Y_{kl} occurs in Eq. (24), we can write

$$\phi_0 = G(t) + D_{00}(t)/r, \quad \epsilon\phi_1 = D_{kl}(t)Y_{kl}/r^{n+1}, \tag{27}$$

where $G(t)$ is kept in order to match with the far-field solution, and $D_{kl}=O(\epsilon)$. Before proceeding to obtain the multipole strengths, we note that at $r>O(R)$, the solution is dominated by volumetric oscillations of the bubble, and the arguments of Lezzi and Prosperetti [10] can be used to match the solution to the far field. In the far field, where spatial coordinates scale with $c_\infty R_c/U$, Eq. (23) reduces to a wave equation, and the bubble is experienced essentially as a standard acoustic source [9,10]. Matching the solutions for ϕ in the inner and outer gives [3]

$$G(t) = \phi_\infty + \frac{\rho}{c_\infty}\frac{d}{dt}(R^2\dot{R}). \tag{28}$$

Here, ϕ_∞ is the potential in the absence of the bubble, and satisfies $\rho\partial\phi_\infty/\partial t=-p_\infty$. We shall return to the inclusion of the last term below.

We first proceed to determine the multipole strengths. The kinematic condition becomes

$$\frac{DF}{Dt} = |[\dot{R} + \dot{R}_{kl}Y_{kl} + D_{00}(t)/r^2 + (k+1)D_{kl}(t)Y_{kl}/r^{k+2}]|_{F=0} = 0, \tag{29}$$

where ( ) indicates differentiation with time. Since $\epsilon \ll 1$ and $D_{kl}/D_{00}=O(\epsilon)$, we can expand the powers of r at $F=0$ into a Taylor series about $r=R(t)$ and ignore products of $O(\epsilon)$ quantities. Using the orthogonality of Y_{kl} (and noting that $Y_{00}=1$), integration of Eq. (29) and Y_{kl} times Eq. (29) then results in

$$D_{00} = -R^2\dot{R}, \quad D_{kl} = -\frac{1}{k+1}R^{k+2}\dot{R}_{kl} - \frac{2}{k+1}R^{k+1}\dot{R}R_{kl}, \tag{30}$$

and D_{kl}/D_{00} is indeed of $O(\epsilon)$, as assumed.

The normal stress boundary condition at the gas-liquid interface is

$$p_g = -\rho\phi_t - \frac{1}{2}\rho|\nabla\phi|^2 + \sigma\nabla\cdot\mathbf{n} - 2\mu\phi_{0,rr} - [\mathbf{nn}:\mathbf{M}]_{R_-}^{R^+} \tag{31}$$

at $F=0$, where σ is the coefficient of surface tension, taken to be constant. The first two terms on the right-hand side of Eq. (31) are obtained by substitution of Eq. (27), evaluating the result at $r=R+R_{kl}Y_{kl}$. The curvature has been obtained by Lamb [17] for small shape oscillations of the form given by Eq. (24),

$$\nabla\cdot\mathbf{n} = \frac{2}{R} + (k+2)(k-1)R_{kl}Y_{kl}/R^2. \tag{32}$$

Upon linearization of Eq. (31) in terms of ϵ,

$$p_g = -\rho\dot{G} - \frac{\rho\dot{D}_{00}}{R}\left(1 - \frac{R_{kl}Y_{kl}}{R}\right) - \frac{\rho\dot{D}_{kl}Y_{kl}}{R^{k+1}} - \frac{\rho}{2}\left[\frac{D_{00}^2}{R^4}\left(1 - \frac{4R_{kl}Y_{kl}}{R}\right) + 2(k+1)\frac{D_{00}D_{kl}Y_{kl}}{R^{k+4}}\right] + \frac{2\sigma}{R} + (k+2)(k-1)\sigma R_{kl}Y_{kl}/R^2 - 4\mu\frac{\dot{R}}{R} - [\mathbf{nn}:\mathbf{M}]_{R_-}^{R^+}. \tag{33}$$

The viscous term in Eq. (31) accounts for the normal stress arising from the spherically symmetric part of the velocity field; viscous effects arising from shape oscillations will be accounted for at the end of this section. The contribution from the Maxwell stress is obtained from Eqs. (16) and (17). Integrating Eq. (33) over a unit sphere, using the orthogonality of surface harmonics, and substitution of D_{00} from Eq. (30) give the modified Rayleigh-Plesset equation,

$$\rho R\ddot{R} + \frac{3}{2}\rho\dot{R}^2 = p_g - p_\infty - \frac{2\sigma}{R} + \frac{R}{c_\infty}(\dot{p}_g - \dot{p}_\infty) - 4\mu\frac{\dot{R}}{R} + \frac{\varepsilon_0\varepsilon}{6}\left((E_0-2A)^2 - 2(E_0+A)^2 + B^2\varepsilon_{\text{in}}/\varepsilon + \left[+\frac{12}{5}A(E_0-5A) - \frac{24}{5}(E_0-2A)(E_0+A) - \frac{24}{5}B^2\varepsilon_{\text{in}}/\varepsilon\right]\frac{R_2}{R}\right), \tag{34}$$

where $p_g=P_o\left(\frac{R_0^3-h^3}{R^3-h^3}\right)^\gamma$ is the gas pressure in which P_o is the external pressure, $h=R_0/8.86$ is the hard-core van der Waals radius, and γ is the polytropic exponent of the gas; $p_\infty = P(t)+P_o$ is the sum of the external pressure and the potentially unsteady forcing pressure, $P(t)=P_a f(t)$, wherein P_a is the forcing pressure amplitude and $f(t)$ is a time-dependent function. In Eq. (34), we have used terms that are of lowest order in c_∞^{-1} to eliminate the last term in Eq. (28). Otherwise, the inclusion of small terms would lead to an increase in the order of the ODE for $R(t)$. Also, we note that additional terms could have been included, within the same order of approximation. Both of these points are reviewed at length in Ref. [3]. We should add that the Mach numbers used in the present paper are very small, and these issues are not expected to be of importance here. The particular choice of the $O(c_\infty^{-1})$ term used in Eq. (34) corresponds to the Rayleigh-Plesset equation in Ref. [14], with which analytical results are compared below, as well as with that in Ref. [18].

The nonspherically symmetric contributions to the dynamic condition are obtained by multiplication of Eq. (33) with Y_{kl}, and subsequent integration over a unit sphere,

$$0 = \frac{\rho \dot{D}_{00} R_{kl}}{R^2} - \frac{\rho \dot{D}_{kl}}{R^{k+1}} + \frac{2\rho D_{00}^2 R_{kl}}{R^5} - (k+1)\frac{\rho D_{00} D_{kl}}{R^{k+4}} + (k+2)(k-1)\sigma R_{kl}/R^2 - \frac{k+1}{\alpha_{kl}} \times \int_0^{2\pi} \int_{-1}^{1} [\mathbf{nn}:\mathbf{M}]_{R_-}^{R^+} Y_{kl}(\mu,\varphi) d\mu d\varphi. \quad (35)$$

Substitution of Eq. (30) and reorganizing shows that the $k=2$, $l=0$ mode has a nonzero contribution from the electric field,

$$\ddot{R}_{20} + 3\frac{\dot{R}\dot{R}_{20}}{R} + \frac{R_{20}}{R}\left(-\ddot{R} + \frac{12\sigma}{\rho R^2}\right) + 8\nu\left[\frac{\ddot{R}_{20}}{R^2}\left(7 - 16\frac{\delta}{R}\right) + \frac{R_{20}\dot{R}}{R^3}\left(1 + 4\frac{\delta}{R}\right)\right] \quad (36)$$

$$= \frac{\varepsilon_0}{\rho R}\left\{\varepsilon[(E_0 - 2A)^2 + (E_0 + A)^2] - 2\varepsilon_{\text{in}}B^2 + \frac{3}{7}\varepsilon[22(E_0 - 2A)A + 10(E_0 + A)A - 4(E_0 - 2A)(E_0 + A) + 12A_3(A - 2E_0)/R^5 + 4B^2\varepsilon_{\text{in}}/\varepsilon + 3BB_3R^2\varepsilon_{\text{in}}/\varepsilon]R_2/R\right\}. \quad (37)$$

For the case $q=0$, $\varepsilon_{\text{in}}=0$, the terms due to the electric field that are proportional to R_{20} can be shown to be equal to their counterparts in Eq. (4.53) of Ref. [1]. The viscous term has been included in a similar manner as in the boundary-layer approximation of Refs. [14,15]. Note that some of the terms in Eqs. (34) and (37) are nonlinear in coefficients of the deformation; these equations will be linearized and rendered dimensionless in the following section.

It can be seen from Eqs. (16) and (17) that there is also a finite contribution from the electric field to an R_{40} mode. This arises if $R_{20} \neq 0$, such that the electric potential has a nonzero P_3 contribution ($A_3 \neq 0$), which, in turn, leads to a P_4 contribution to the Maxwell stress. However, there is no possibility of any feedback from an R_{40} mode into the R_{20} mode in the present analysis, which is linear in R_{kl}. We shall study the evolution of R_{20} primarily as a check on the assumption that the deformation of the bubble remains small during the numerical simulations. For other combinations of k and l,

$$\ddot{R}_{kl} + 3\frac{\dot{R}\dot{R}_{kl}}{R} + \frac{R_{kl}}{R}\left((1-k)\ddot{R} + \frac{(k+2)(k+1)(k-1)\sigma}{\rho R^2}\right) = 0, \quad (38)$$

in agreement with Ref. [14], and there is no effect of the electric field.

C. Dimensionless equations

We render the ordinary differential equations for R and R_{20} dimensionless by using the following scalings:

$$(R, R_{20}) = R_c(\tilde{R}, \widetilde{R_{20}}) = R_o(\tilde{R}, \widetilde{R_{20}}), \quad \mathbf{u} = \left(\frac{\sigma}{\rho R_o}\right)^{1/2}\tilde{\mathbf{u}}, \quad t = \left(\frac{\rho R_o^3}{\sigma}\right)^{1/2}\tilde{t}, \quad p = \left(\frac{\sigma}{R_o}\right)\tilde{p},$$

$$E_0 = E_{oo}\tilde{E}_0, \quad q = (\varepsilon\varepsilon_0 E_{oo})\tilde{q}, \quad (39)$$

where tildes signify dimensionless quantities. Here, R_o and E_{oo} represent an equilibrium bubble radius and average electric-field strength, respectively. Substitution of these scalings into Eqs. (34) and (37) yields (following the suppression of the tilde decoration)

$$R\ddot{R} + \frac{3}{2}\dot{R}^2 = p_g - p_\infty - \frac{2}{R} + \text{Ma}(\dot{p}_g - \dot{p}_\infty) - 4\text{Oh}\frac{\dot{R}}{R} + \frac{\text{W}}{6}\left(2A^2 - 8AE_0 - E_0^2 + \lambda B^2 - \frac{6R_2}{5R}(8A_0^2 - 6E_0A_0 + 4E_0^2 + 4\lambda B_0^2)\right), \quad (40)$$

$$\ddot{R}_{20} + 3\frac{\dot{R}\dot{R}_{20}}{R} + \frac{R_{20}}{R}\left(-\ddot{R} + \frac{12}{R^2}\right) + \frac{8\text{Oh}}{R^2}\left[\dot{R}_{20}\left(7 - 16\frac{\delta}{R}\right) + \frac{R_{20}}{R}\dot{R}\left(1 + 4\frac{\delta}{R}\right)\right] = \frac{\text{W}}{R}\left(5A_0(A_0 + 2A_1) - 2E_0(A_0 + A_1) + 2E_0^2 - 2\lambda B_0(B_0 + 2B_1) - \frac{6}{7}\frac{R_{20}}{R}(13A_0^2 - 18E_0A_0 + 2E_0^2 - 2\lambda B_0^2)\right). \quad (41)$$

Here, $p_g = \Pi_o\left(\frac{1-H^3}{R^3-H^3}\right)^\gamma$ is the dimensionless gas pressure and $P(t) = \Pi_a f(t)$ is the dimensionless forcing pressure in which $\Pi_a = \Pi_o - 2$, whence $p_\infty = (\Pi_o - 2)[1 + f(t)]$; we shall take $f(t) = -\sin(\Omega t)$, where $\Omega \equiv \omega(\rho R_0^3/\sigma)^{1/2}$ is a dimensionless forcing frequency.

The dimensionless equations for the interfacial charge density are expressed by

$$-\dot{\hat{q}} = K(E_0 - 2A) - K_{\text{in}}B + 2\hat{q}\frac{\dot{R}}{R} + \frac{6R_{20}}{5R}\left(K(A_0 - E_0) + K_{\text{in}}B_0 + \frac{4}{3}\frac{\dot{R}}{R}\hat{q}\right) + \frac{4\hat{q}}{5R}\dot{R}_{20}, \quad (42)$$

$$-\dot{\hat{q}}_3 = \frac{6R_{20}}{5R}\left(K(E_0 + 4A_0) - K_{\text{in}}B_0 + 2\frac{\dot{R}}{R}\hat{q}\right) + 2\frac{\dot{R}}{R}\hat{q}_3 - 4K\frac{A_3}{R^5} - 3K_{\text{in}}B_3R^2. \quad (43)$$

In the above equations, the dimensionless functions $A = A_0 + A_1$, $B = B_0 + B_1$, A_3/R^5, and B_3R^2 are given by

$$A_0 \equiv \frac{E_0(1-\lambda) - \hat{q}}{\lambda + 2}, \quad (44)$$

$$A_1 \equiv \frac{2}{5(\lambda+2)^2}\frac{R_{20}}{R}[-3(\lambda-1)^2E_0 - 3(2\lambda+1)\hat{q}], \quad (45)$$

$$B_0 \equiv \left(\frac{3E_0-\hat{q}}{\lambda+2}\right), \quad (46)$$

$$B_1 \equiv B_0\left(\frac{6(\lambda-1)}{5(\lambda+2)}\frac{R_{20}}{R}\right), \quad (47)$$

$$\frac{A_3}{R^5} = \frac{1}{3\lambda+4}\left(\frac{3R_{20}}{5R}[(2-3\lambda)E_0 - \lambda B_0 + 2A_0(3\lambda+4)] - \hat{q}_3\right), \quad (48)$$

$$B_3R^2 = \frac{1}{3\lambda+4}\left(\frac{6R_{20}}{5R}[3E_0 - (\lambda+2)B_0] - \hat{q}_3\right). \quad (49)$$

Note that $A^2 \approx A_0(A_0+2A_1)$ and $B^2 \approx B_0(B_0+2B_1)$. Here, A and B were scaled on E_{oo}, and A_3 and B_3 on $E_{oo}R_0^5$ and E_{oo}/R_0^2, respectively. The dimensionless parameters that appear in the above equations are defined as follows:

$$\mathrm{Oh} \equiv \frac{\mu}{(\rho\sigma R_0)^{1/2}}, \quad \mathrm{Ma} \equiv \frac{(\sigma/\rho R_0)^{1/2}}{c_w}, \quad \mathrm{W} \equiv \frac{\varepsilon\varepsilon_0 E_{00}^2}{\sigma/R_0},$$
$$(K, K_{\mathrm{in}}) \equiv \frac{(\rho R_0^3/\sigma)^{1/2}}{\varepsilon\varepsilon_0/(\kappa, \kappa_{\mathrm{in}})}, \quad \lambda \equiv \varepsilon_{\mathrm{in}}/\varepsilon, \quad (50)$$

which correspond to an Ohnesorge number, a Mach number, a parameter reflecting the relative importance of electric effects to surface tension forces, dimensionless conductivities, and a ratio of dielectric constants, respectively; the dimensionless thickness of the boundary layer around the bubble in which vorticity effects are confined is $\delta = \min((\mathrm{Oh}/\Omega)^{1/2}, R/4)$ and the dimensionless external and forcing pressures are $(\Pi_o, \Pi_a) \equiv (P_o, P_a)R_0/\sigma$. Note that the applied electric field can potentially be time-dependent, that is, $E_0 = E_0(t)$, and the effect of this feature on the bubble dynamics will be explored in the following section. In what follows, the hat decoration will be suppressed henceforth and we shall also take $R_{20} \to R_2$ and $E_0 \to E$.

This is clearly a parameterically rich problem. We therefore restrict the present work to an investigation of the parameters related to the presence of an electric field: W, λ, K_{in}, and K (as well as the specific form of the time dependence of the applied electric field) in addition to Π_o and Ω on the bubble and charge dynamics. The remaining parameters will be held constant: $H=0.113$, $\gamma=1$, $\mathrm{Ma}=1.81\times10^{-3}$, and $\mathrm{Oh}=0.037$; these were obtained for the following choice of physical parameters: $R_0=10^{-5}$ m, $\mu=10^{-3}$ Pa s, $\rho=10^3$ Kg/m^3, $\sigma=0.073$ mN/m, and $c_w=1481$ m/s. Note that these parameters are typical for a conducting liquid such as water, and the majority of the results presented below will be in the limit of high conductivity and large difference in dielectric constants between the gas and liquid phases. Numerical solutions of the ordinary differential equations governing $R(t)$ and $R_2(t)$, $q(t)$ and $q_3(t)$ are obtained using Gear's method. The predictions of the numerical procedure were validated against solutions obtained using MATHEMATICA. Solutions obtained in previous work were also reproduced by the numerical procedure employed, which inspires further confidence in its predictions. The numerical results are presented next.

III. RESULTS

Here, we present a discussion of our results. The results generated for the case of a constant electric field are presented first, followed by those obtained for time-dependent fields. Cases involving combinations of time-dependent electric fields and external pressure forcing are also considered.

A. Steady-state solutions

We begin the presentation of our results by examining the effect of varying the dimensionless strength of the externally applied electric field, W, on the steady solutions for R and R_2 in the limit of small λ and K_{in}/K. As shown in Fig. 1, in which we plot the variation of the steady solutions for R and R_2 with W for different values of Π_o, increasing W results in a decrease in R and an increase in the degree of bubble deformation. The departure of R from unity is also seen to increase and the magnitude of R_2 decreases with decreasing Π_o. As also shown in Fig. 1, the magnitude of R and R_2 associated with finite values of λ and K_{in}/K is larger for the range of Π_o and W shown; this indicates that, over this range, decreasing the difference in dielectric constant and conductivity between the two phases is stabilizing against bubble contraction.

We have also examined the dependence of the steady solutions for q on the relevant system parameters. In Fig. 2, we show the variation of q with λ for different values of the ratio K_{in}/K. For a given K_{in}/K ratio, the magnitude of q increases with decreasing λ, which corresponds to a decrease in the ratio of the dielectric constants of the two phases. For small λ values, q increases with K_{in}/K while for negligible K_{in}/K, the magnitude of q becomes zero-valued; that is, in the limit of large liquid conductivity and electric permittivity, the time scale associated with interfacial charge relaxation becomes so small that it becomes exceedingly difficult to sustain the presence of interfacial charge. The results presented in the remaining sections of the present work have largely been generated in this limit.

The behavior exhibited by R and R_2 in Fig. 1 and q in Fig. 2 can be understood by assuming that $(R_2/R, q_3) \ll 1$, $H^3 \ll 1$, and considering the steady version of Eqs. (40)–(43) in the limit of small λ,

$$\frac{\Pi_o}{R^{3\gamma}} - p_\infty - \frac{2}{R} - \frac{3}{4}\left[\left(1-\frac{3\lambda}{2}\right) - \frac{(2-\lambda)}{3}q\left(1+\frac{q}{6}\right)\right]W \sim 0, \quad (51)$$

$$q \sim \frac{3}{2\left(1+\frac{K_{\mathrm{in}}}{2K}\right)}\left[\left(\frac{K_{\mathrm{in}}}{K}\right) - \lambda\right]. \quad (52)$$

A limiting formula for R_2 can also be determined for small λ, which is expressed in terms of λ, K_{in}, K, and W as follows:

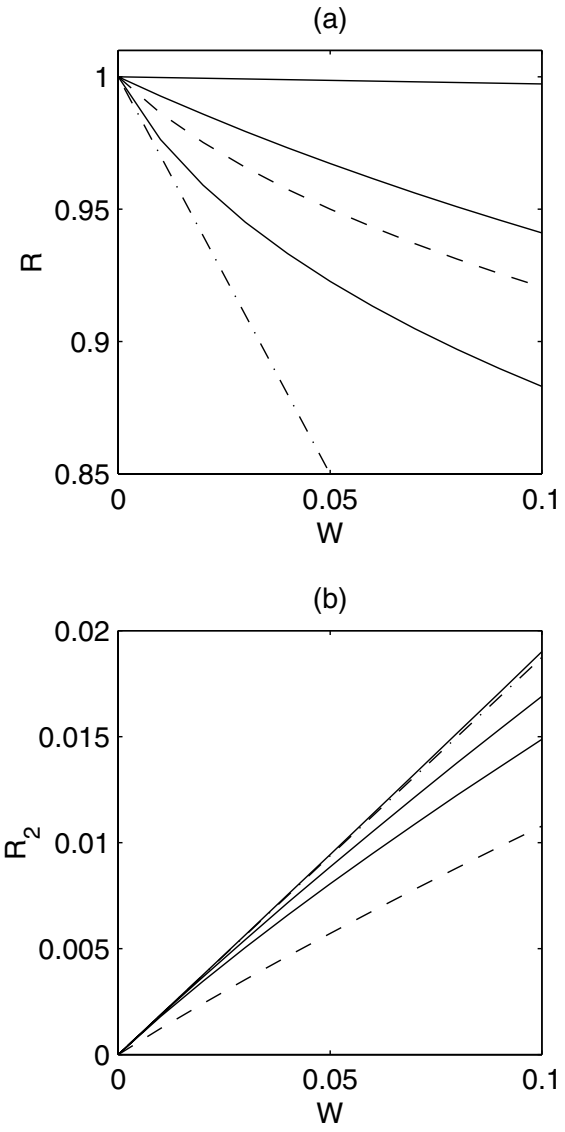

FIG. 1. The effect of varying W on the steady solutions for R and R_2 for different Π_o. The solid curves from top to bottom in panels (a) and (b) have $\Pi_o=10$, 1, and 0.75. The dashed curves in (a) and (b) were generated with $\Pi_o=0.75$, $\lambda=0.1$, and $K_{\text{in}}/K_{\text{out}}=0.5$. The dot-dashed lines in (a) and (b) represent $R=1-(3/4W)/(3\gamma\Pi_o-2)$ (with $\gamma=1$ and $\Pi_o=0.75$) and $R_2=3W/16$, respectively. The rest of the parameters are $\gamma=1$ and $H=0.113$.

$$R_2 \sim \frac{21\{2\lambda-(1+[K_{\text{in}}/K]^2)\}W}{-28(2+[K_{\text{in}}/K])^2+6([5+6\lambda]-11[K_{\text{in}}/K]^2)W}. \tag{53}$$

The limiting formula for q, given by Eq. (52), is in agreement with the solutions shown in Fig. 2 for small λ values. Furthermore, if K_{in}/K is greater (less) than λ, then q is positive (negative), which is also in accordance with the numerical solutions shown in Fig. 2. The above limiting relations can also be used to understand the influence of interfacial charges arising from a contrast in dielectric constants and conductivities on the bubble radius and deformation. Upon

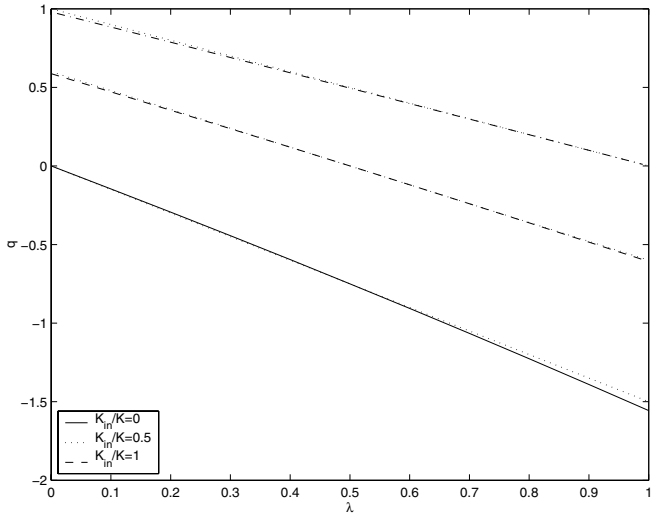

FIG. 2. The effect of varying λ on the steady solutions for q for $K_{\text{in}}/K=0$, 0.5, and 1. The dotted lines represent steady solutions for q obtained using the limiting formula given by Eq. (52). The rest of the parameter values remain unchanged from Fig. 1.

inspection of Eq. (51), it is seen that the electric contribution can be of the same sign as the surface tension term, which promotes a transition to smaller bubble radii, if certain conditions are satisfied. These conditions can be determined by examining Eq. (51) in the limit $R-1\ll 1$,

$$R-1\equiv\delta R\sim-\frac{3}{4}\frac{\left[\left(1-\frac{3\lambda}{2}\right)-\frac{(2-\lambda)}{3}q\left(1+\frac{q}{6}\right)\right]}{(3\gamma\Pi_o-2)}W. \tag{54}$$

We look for conditions under which $\delta R<0$. For $\lambda\ll 1$, the steady interfacial charge and δR become

$$q\sim\frac{3}{2\left(2+\frac{K_{\text{in}}}{2K}\right)}\frac{K_{\text{in}}}{K},\quad \delta R\sim-\frac{3}{4}\frac{\left[1-\frac{2}{3}q\left(1+\frac{q}{6}\right)\right]}{(3\gamma\Pi_o-2)}W. \tag{55}$$

For $\Pi_o>2/3\gamma$, $\delta R<0$ since $q>0$ (provided q is sufficiently small), implying that the bubble contracts; however, δR becomes less negative with increasing q, which indicates that although the effect of the electric field is to promote bubble collapse, the presence of interfacial charge is stabilizing in this case; this is in agreement with the solutions shown in Fig. 1 [see the dashed curve for $\Pi_o=0.75$, $\lambda=0.1$, and $K_{\text{in}}/K=0.5$ in Fig. 1(a), which overlies that associated with that for $\Pi_o=0.75$ and $\lambda=K_{\text{in}}/K=0$]. If $\Pi_o<2/3\gamma$, then $\delta R<0$ provided $2q(1+q/6)/3>1$. For $K_{\text{in}}/K\ll 1$, δR and q read

$$q \sim -\frac{3\lambda}{2}, \quad \delta R \sim -\frac{3}{4}\frac{\left[1-\frac{3\lambda}{2}+\lambda\frac{(2-\lambda)}{2}\left(1-\frac{\lambda}{4}\right)\right]}{(3\gamma\Pi_o-2)}W. \tag{56}$$

However, λ is expected to be small in practical applications, thus $\delta R \sim -3(1+\lambda)/4(3\gamma\Pi_o-2)$, suggesting that the presence of charge is destabilizing (stabilizing) for $\Pi_o > 2/3\gamma$ ($\Pi_o < 2/3\gamma$) in this limit.

In the limit of small gas conductivity and dielectric constant, which is most appropriate for the present work, $(\lambda, K_{\text{in}}/K) \ll 1$, and Eqs. (52)–(54) and reduce to

$$q \sim 0, \quad R_2 \sim \frac{3}{16}W, \quad \delta R = -\frac{\frac{3}{4}W}{3\gamma\Pi_o-2}; \tag{57}$$

these limiting relations are in agreement with Eq. (3.21) in Ref. [1]. Inspection of Fig. 1 also reveals close agreement between the predictions of Eqs. (57) and the steady solutions for R and R_2 in the limit of small W. As has been pointed out in Ref. [1], inspection of Eq. (57) suggests that the application of an electric field can lead to bubble contraction or expansion depending on whether $\Pi_o > 2/3\gamma$ or $< 2/3\gamma$, respectively. This equation also explains why $R \to 1$ for large Π_o and the occurrence of two branches of solutions in Fig. 3(a), in which we show the dependence of steady solutions for R on Π_o for different W values. However, it is seen from Fig. 3(a) that the singular point $\Pi_o = 2/3\gamma$ is replaced by the tilted dashed line (corresponding to $W=0$) when the full equations of motion are solved. It is clear from Eq. (40) that, at steady state and $\gamma=1$, if p_g is not linearized in terms of $R-1$, a fourth-order polynomial results for R, with multiple solutions for a given value of Π_o. The significance of the observation that multiple steady states are possible in the present formulation will aid us in understanding results under unsteady conditions. Here, we add that Fig. 3(b) shows that the degree of deformation of the bubble increases when the relative significance of the applied electric field increases.

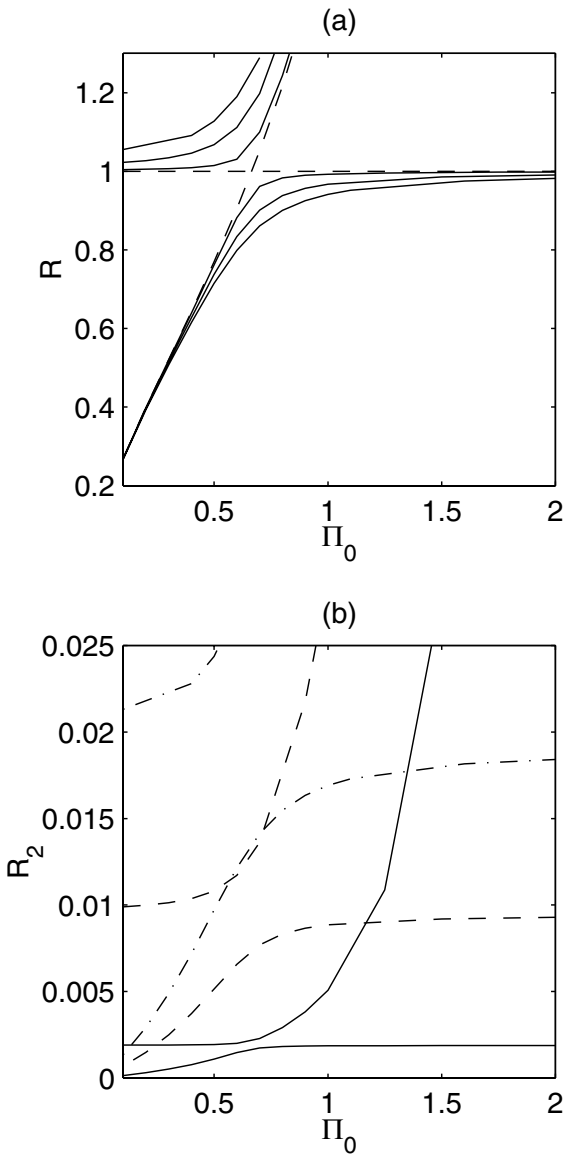

FIG. 3. The effect of varying Π on the steady solutions for R and R_2 for different W. The curves below $R=1$ in panel (a) from top to bottom have $W=0.01$, 0.05, and 0.1. In panel (b), the solid, dashed, and dot-dashed lines have $W=0.01$, 0.05, and 0.1, respectively. The rest of the parameter values remain unchanged from Fig. 1.

B. Time-dependent bubble size and shape in a stationary electric field

Here, we investigate the effect of initial conditions on the bubble dynamics, including the effect of instantaneously switching on an electric field. In Fig. 4, we show the temporal variation of $R(t)$ and $R_2(t)$ for $W=0.11$, Oh=0.037, Ma $=1.81\times10^{-3}$, $\Pi_o=137$, $(K, K_{\text{in}})=(4.65\times10^{-3}, 0)$, $H=0.113$, $\gamma=1$, and in the limit $\lambda \to 0$. For all cases considered, $R(t)$ is seen to undergo oscillations whose amplitude decays with increasing time; the decay rate appears to increase with the initial value of R [see Fig. 4(a)]. As shown in Fig. 4(b), the bubble deformation, characterized by R_2, becomes increasingly significant with time for a sufficiently large initial bubble radius, even though the amplitude of R decreases. The increase in R_2 appears to be cumulative, although qualitatively constant. In fact, for $R(0)=2$, $R_2=O(1)$ for $t=O(1)$, which renders the present theory invalid. These results will be related to the bubble dynamics observed during so-called "after-bounces" in the presence of an electric field in subsequent sections.

We investigate next a case in which an electric field is suddenly switched on at $t=0$. In Fig. 5, we show the dependence of $R(t)$ and $R_2(t)$ on Π_o with the rest of the parameters remaining unchanged from Fig. 4. As shown in Fig. 5(a), at relatively large values of the external pressure (see the curve associated with $\Pi_o=1.37$) the bubble radius, $R(t)$, undergoes small-amplitude oscillations that appear to decay with time. Decreasing Π_o, however, results in bubble collapse, characterized by a sharp decrease in $R(t)$ with time, followed by several "after-bounces," before a new, steady value of R is reached. These dynamics can be understood by referring to

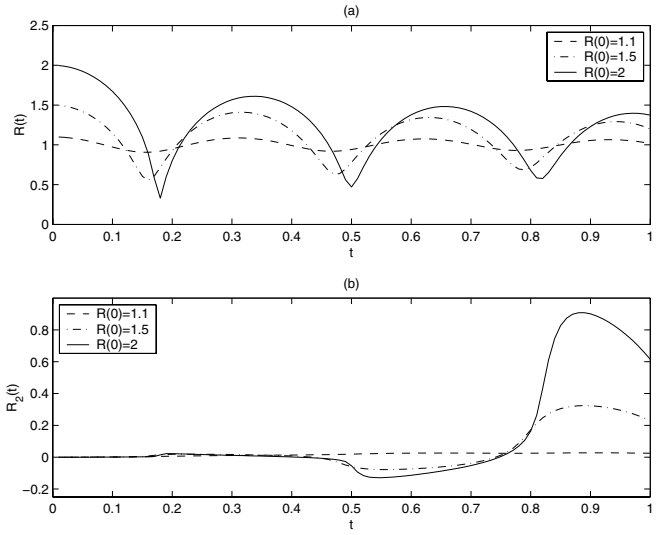

FIG. 4. The effect of varying the initial conditions on the solution for $R(t)$ and $R_2(t)$ with $W=0.11$, Oh=0.037, Ma$=1.81\times10^{-3}$, $\Pi_o=13.7$, $\lambda=0$, and $(K,K_{\text{in}})=(4.67\times10^{-3},0)$. The rest of the parameters are the same as in Fig. 1.

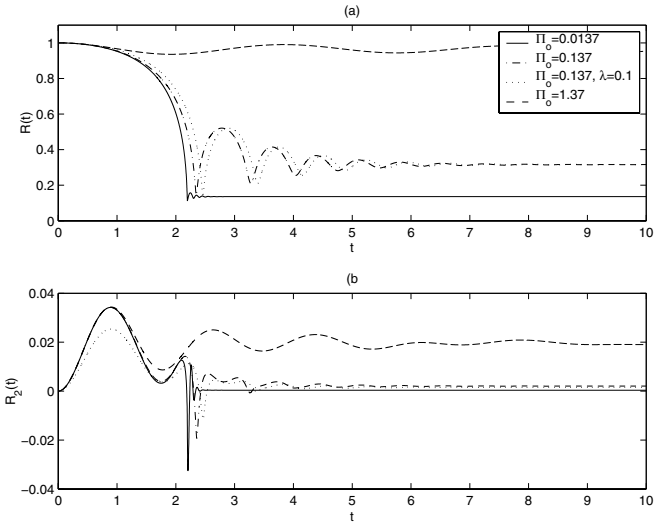

FIG. 5. The effect of varying Π_o on the solution for $R(t)$ and $R_2(t)$. The rest of the parameters remain unchanged from Fig. 4.

Fig. 3. For small values of Π_o, the steady value of R undergoes a substantial decrease with decreasing Π_o. The collapse exhibited by $R(t)$ starting from $R(0)=1$ for $\Pi_o=0.137$ in Fig. 5(a) is an attempt at reaching a steady value of $R\sim0.316\,070$. This collapse, however, is accompanied by an overshoot, which is then followed by an expansion phase; this expansion is, in turn, followed by another collapse, albeit to a shallower minimum in R, and these after-bounces are repeated until the steady state is reached. The after-bounces resemble the dynamics exhibited by $R(t)$ in Fig. 4(a). Upon decreasing the value of Π_o to $\Pi_o=0.0137$, the bubble radius undergoes a more rapid collapse to a steady value of $R\sim0.135\,826$, punctuated by a very short period of after-bounces that are of much smaller amplitude than those associated with the $\Pi_o=0.137$ case. The development of R_2, which achieves relatively small magnitudes, follows the evolution of R closely: for relatively large Π_o, R_2 exhibits oscillations that decay to a steady value, which is in agreement with the solutions shown in Fig. 3(b). For smaller Π_o values, R_2 achieves progressively smaller steady values via decaying oscillations, which coincide with the after-bounces observed in $R(t)$, and whose frequency increases with decreasing Π_o.

The effect of finite λ was also briefly investigated. Examination of Fig. 5, in which we show solutions for R and R_2 for $\lambda=0.1$ and $\Pi_o=0.137$ (with the rest of the parameters remaining unaltered), reveals that the rate of collapse diminishes slightly with increasing λ, that is, for a decreasing contrast in the dielectric constants of the two phases. The steady value reached for R is also slightly larger, $R\sim0.316\,114$, for $\lambda=0.1$. This can be explained by examining the differential equations that describe the bubble dynamics for small λ and $(R_2,q_3)\ll1$. The steady solution for q in this case is given by Eq. (52), which when substituted into Eq. (40) yields the following relation for the steady solution for R in these limits ($R\gg H$ and $H\ll1$ was also assumed here),

$$\frac{\Pi_o}{R^{3\gamma}}-\frac{2}{R}\sim\Pi_o-2+\frac{3}{2\left(2+\frac{K_{\text{in}}}{K}\right)^2}\left(2-\lambda-\left[\frac{K_{\text{in}}}{K}\right]^2\right)W. \tag{58}$$

Inspection of this equation suggests that an increase in the value of λ or the ratio of conductivities gives rise to an increase in R at steady state. This, in turn, suggests that the presence of charge at the interface exerts a stabilizing influence against bubble collapse.

C. Time-dependent electric field

Next, we study the effect of a time-dependent electric field on the bubble dynamics while keeping Π_o constant. Here, we set $E(t)=\sin(\Omega t)$ and obtain solutions for $R(t)$ and $R_2(t)$ for $W=0.11$, 0.69, and 0.99, $\Pi_o=1.39$, and $\Omega=0.62$; the rest of the parameters remain unchanged from Fig. 5. As shown in Fig. 6(a), for the smallest value of W investigated, both $R(t)$ and $R_2(t)$ exhibit sustained small-amplitude oscillations about $R=1$. The frequency of these oscillations appears to be approximately twice that of the applied field, Ω, as would be anticipated from the fact that the Maxwell stress is proportional to E_{oo}^2. With increasing W, the response of $R(t)$ and $R_2(t)$ becomes nonlinear, with the degree of nonlinearity increasing with W. The difference in frequency in the oscillations in the electric field and R is expected to result in other frequencies being introduced, due to the nonlinear dependencies of the Maxwell stress on both functions. At $W=0.99$, it appears that oscillations at two distinct frequencies occur: one that is roughly twice the imposed frequency of the time-dependent electric field and another, larger frequency. This is particularly prominent in the dynamics of R_2 shown in Fig. 6(c). For a sufficiently large value of W, our results indicate that the amplitude of the bubble oscillations becomes so large that it gives rise to bubble collapse followed by an after-bounce phase (not shown). This is, however, ac-

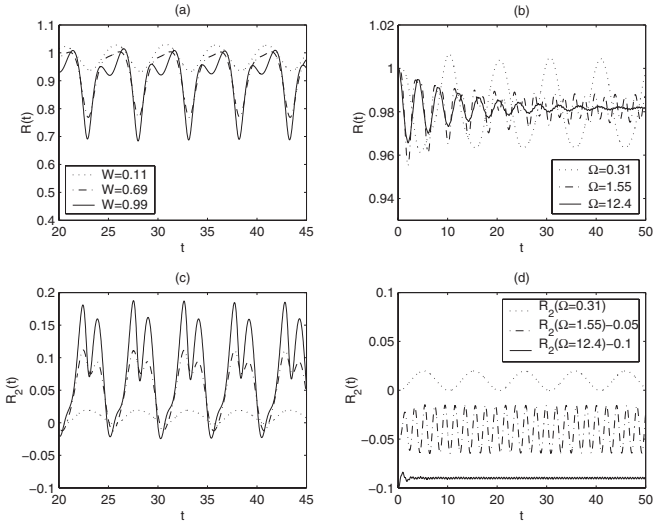

FIG. 6. The effect of varying W and Ω on the solution for $R(t)$ and $R_2(t)$, shown in (a) and (c) and (b) and (d), respectively. In (a) and (c), $E(t)=\sin(\Omega t)$, $\Pi_o=1.39$, and $\Omega=0.62$; in (b) and (d), $E(t)=\sin(\Omega t)$ and $W=0.11$. The rest of the parameters remain unchanged from Fig. 4.

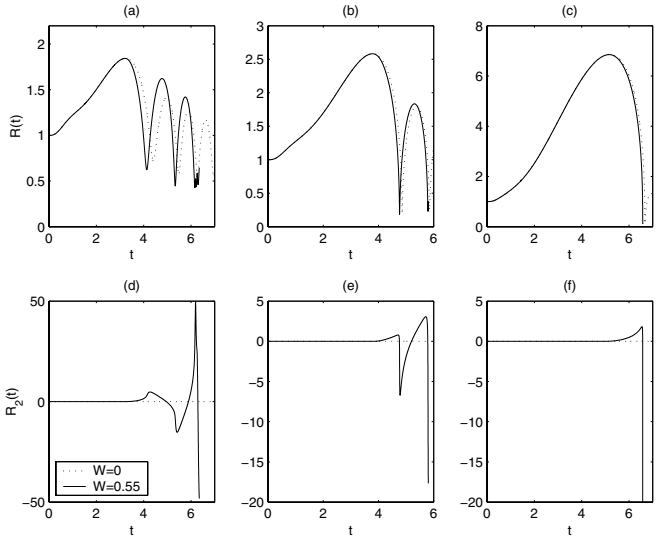

FIG. 7. The effect of varying W on the solution for $R(t)$ and $R_2(t)$ with time-dependent pressure and electric-field forcing. (a) and (d) $P(t)=-0.85\Pi_a \sin(\Omega t)$, $E(t)=(1/2)(\tanh[30(t-3.2)]-\tanh[30(t-4)])$; (b) and (e) $P(t)=-\Pi_a \sin(\Omega t)$, $E(t)=(1/2)(\tanh[30(t-3.8)]-\tanh[30(t-4.2)])$; (c) and (f) $P(t)=-1.5\Pi_a \sin(\Omega t)$, $E(t)=(1/2)(\tanh[30(t-5)]-\tanh[30(t-6)])$. $\Omega=0.62$, $\Pi_0=13.7$ and the rest of the parameters remain unchanged from Fig. 4.

companied by large deformations that render our theory invalid.

We have also investigated the effect of varying the frequency of the applied electric field, Ω, on the dynamics. In Figs. 6(b) and 6(d), we show solutions for $R(t)$ and $R_2(t)$ for $\Omega=0.3331$, 1.55, 12.4, and $W=0.11$, with the rest of the parameters remaining unchanged from Fig. 5. As can be clearly seen, the frequency of the oscillations in both $R(t)$ and $R_2(t)$ is approximately equal to 2 Ω at the lowest frequencies studied. At higher Ω, "phase-locking" appears to take place: the frequency of oscillation of $R(t)$ and $R_2(t)$ adjusts from relatively low values to the imposed frequency of the applied electric field.

D. Time-dependent external pressure and an electric field

Here, we investigate the effect of having a time-dependent external pressure on the behavior of the bubble, $P(t)=-\Pi_a \sin(\Omega t)$, where Π_a is the amplitude of the pressure forcing. In Figs. 7(b) and 7(e), we show the response of $R(t)$ and $R_2(t)$ to the time-dependent pressure forcing with $\Pi_a=1$, $\Omega=0.62$, $\Pi_o=13.7$ in the presence of a time-dependent electric field, $E(t)=\frac{1}{2}(\tanh[30(t-t_1)]-\tanh[30(t-t_2)])$, characterized by $W=2.75$ as well as in its absence; the rest of the parameters remain unchanged from Fig. 5. The external pressure decreases over the first quarter of the forcing cycle and the bubble, which remains essentially undeformed, undergoes expansion, as shown in Fig. 7(b). During the second quarter of the cycle, the external pressure increases, which drives the rapid collapse of the bubble to relatively small values of $R(t)$; this is then followed by a phase dominated by after-bounces. In the absence of electric forcing, the collapse is accompanied by negligible deformation and the after-bounces eventually lead to another expansion phase followed by collapse, etc. For $W=0.55$, the time-dependent electric field is switched on at $t=t_1=3.8$ and switched off at $t=t_2=4.2$ such that it remains active over the period during which the bubble is at the end of the expansion phase. The application of $E(t)$ appears to give rise to an increase in the rate of collapse, which implies that an electric field may be used to accelerate bubble collapse thereby giving rise to even more intense conditions within the bubble. This may be of interest in some applications, such as sonoluminescence (e.g., Ref. [14]), or in attempts to achieve fusion [5]. As shown in Fig. 7(e), however, the magnitude of R_2 becomes $O(10)$ during the collapse and subsequent after-bounce stage, which invalidates the present theory; we therefore halt our simulations at this point. The amplification of the bubble deformation during the after-bounces is seen to be very similar to that in Fig. 4 for a bubble in a steady electric field.

We have also investigated the effect of varying the amplitude of the pressure forcing on the bubble dynamics, with a view to accelerating further the rate of bubble collapse. We show in Figs. 7(a) and 7(d) solutions for $R(t)$ and $R_2(t)$ for $\Pi_a=0.85$ and $E(t)=\frac{1}{2}(\tanh[30(t-3.2)]-\tanh[30(t-4)])$ with the rest of the parameters remaining unaltered from Figs. 7(a) and 7(d). As shown in panel (a) of Fig. 7, this leads to a marked acceleration in the collapse rate of the bubble, accompanied by moderate deformation. The magnitude of the deformation characterized by R_2, however, increases significantly during the after-bounce stage of the dynamics, which, once again, invalidates our theory at later times, leading us to halt the simulations. We have also found that increasing the amplitude of the pressure forcing, Π_a, results in larger collapse rates, which are accelerated further in the presence of a time-dependent electric field, as shown in Figs. 7(c) and 7(f), which was generated with $\Pi_a=1.5$.

IV. CONCLUSIONS

We have examined the effect of a homogeneous, irrotational, solenoidal, and unsteady electric field on the collapse of a gas bubble in a liquid. We have presented an analysis describing the bubble dynamics that accounts for electric contributions, which enter the problem through the interfacial boundary conditions. The latter were obtained by solving the corresponding electrostatic problem. Elliptical shape oscillations were also accounted for, but assumed to be small. The analysis resulted in a modified Rayleigh-Plesset-type equation for the bubble radius, coupled to ordinary differential equations for the bubble deformation and the interfacial charge-density distribution. Our theory extends previous work by Lee and Kang [1] for small volumetric and shape oscillations of bubbles into the nonlinear regime.

Numerical solutions of the derived set of equations demonstrated clearly that electric fields have significant effects on the dynamics of collapsing bubbles. For example, the results presented in Fig. 5 show that, within the approximations made here, a bubble can be made to collapse by suddenly switching on an electric field. This is caused by a multiplicity of possible steady states at sufficiently low values of the ambient pressure. A harmonic electric field results in volumetric oscillations at approximately twice the frequency of the applied field for weak amplitudes and at competing frequencies for stronger fields. Further, it was seen that the collapse of a bubble driven by variations in the ambient pressure can be accelerated by using a pulsed electric field, which is switched on and off at the end of the expansion phase of the bubble; this result may be of significance for applications such as sonoluminescence [3] and nanoscale thermonuclear fusion [5]. However, the results indicate that, during after-bounces, the bubble deformation accumulates.

As with the well-documented Rayleigh-Plesset equation (e.g., Ref, [9]), the theory is limited to small Mach and large Reynolds number values. For systems in which the Mach number is relatively large, full numerical simulations are necessary (e.g., Ref. [5,19]).

ACKNOWLEDGMENT

The authors would like to thank the EPSRC for their support through Grant No. EP/D50371X/1 and Dr. Stephen J. Shaw for carefully checking the analysis.

[1] S. M. Lee and I. S. Kang, J. Fluid Mech. **384**, 59 (1999).
[2] M. Ward, J. Wu, and J.-F. Chiu, Ultrasound Med. Biol. **26**, 1169 (2000).
[3] M. P. Brenner, S. Hilgenfeldt, and D. Lohse, Rev. Mod. Phys. **74**, 425 (2002).
[4] M. S. Plesset and A. Prosperetti, Annu. Rev. Fluid Mech. **9**, 145 (1977).
[5] R. I. Nigmatulin, I. Sh. Akhatov, A. S. Topolnikov, R. Sh. Bolotnova, N. K. Vakhitova, R. T. Lahey, and R. P. Taleyarkhan, Phys. Fluids **17**, 107106 (2005).
[6] T. B. Jones and G. W. Bliss, J. Appl. Phys. **48**, 1412 (1977).
[7] Z. Z. Yin and A. Prosperetti, J. Micromech. Microeng. **15**, 643 (2005).
[8] P. Di Marco, W. Grassi, G. Memoli, T. Takamasa, A. Tomiyama, and S. Hosokawa, Int. J. Multiphase Flow **29**, 559 (2003).
[9] A. Prosperetti and A. Lezzi, J. Fluid Mech. **168**, 457 (1986).
[10] A. Lezzi and A. Prosperetti, J. Fluid Mech. **185**, 289 (1986).
[11] V. I. Kushch, A. S. Sangani, P. D. M. Spelt, and D. L. Koch, J. Fluid Mech. **460**, 241 (2002).
[12] D. A. Saville, Annu. Rev. Fluid Mech. **29**, 27 (1997).
[13] H. A. Stone, Phys. Fluids A **2**, 111 (1990).
[14] S. Hilgenfeldt, D. Lohse, and M. P. Brenner, Phys. Fluids **8**, 2808 (1996).
[15] M. P. Brenner, D. Lohse, and T. F. Dupont, Phys. Rev. Lett. **75**, 954 (1995).
[16] A. Prosperetti, Q. Appl. Math. **34**, 339 (1977).
[17] H. Lamb, *Hydrodynamics* (Cambridge University Press, Cambridge, UK, 1932).
[18] S. J. Putterman and K. R. Weninger, Annu. Rev. Fluid Mech. **32**, 445 (2000).
[19] W. C. Moss, D. B. Clarke, J. W. White, and D. A. Young, Phys. Fluids **6**, 2979 (1994).